Accepted Manuscript

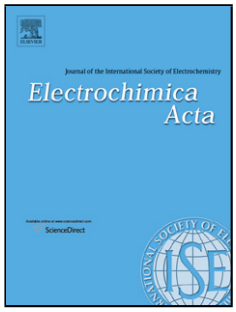

Title: Structure and Transport in Coatings from Multiscale Computed Tomography of Coatings—New Perspectives for Eelectrochemical Impedance Spectroscopy Modeling?

Author: A.E. Hughes A. Trinchi F.F. Chen YS. Yang S. Sellaiyan J. Carr P.D. Lee G.E. Thompson T.Q. Xiao

PII: S0013-4686(15)30759-3
DOI: http://dx.doi.org/doi:10.1016/j.electacta.2015.10.183
Reference: EA 25987

To appear in: *Electrochimica Acta*

Received date: 30-8-2015
Revised date: 29-10-2015
Accepted date: 29-10-2015

Please cite this article as: A.E.Hughes, A.Trinchi, F.F.Chen, YS.Yang, S.Sellaiyan, J.Carr, P.D.Lee, G.E.Thompson, T.Q.Xiao, Structure and Transport in Coatings from Multiscale Computed Tomography of CoatingsmdashNew Perspectives for Eelectrochemical Impedance Spectroscopy Modeling?, Electrochimica Acta http://dx.doi.org/10.1016/j.electacta.2015.10.183

Structure and Transport in Coatings from Multiscale Computed Tomography of Coatings – New Perspectives for Eelectrochemical Impedance Spectroscopy Modeling?

A. E. Hughes[1,2], A. Trinchi[3], F. F. Chen[3], Y. S. Yang[3], S.Sellaiyan[4], J. Carr[5], P.D. Lee[5], G.E. Thompson[5] and T. Q. Xiao[6]

[1]Institute for Frontier Materials, Deakin University, Waurn Ponds, Geelong, Australia
[2]CSIRO Minerals Resources, Clayton, 3169, Australia
[3]CSIRO Manufacturing, Private Bag 10 Clayton, 3169, Australia
[4]Division of Applied Physics, University of Tsukuba, Ibaraki 305-8577, Japan
[5]School of Materials, The University of Manchester, Manchester M13 9PL, England, UK.
[6]Shanghai Institute of Applied Physics, Chinese Academy of Sciences, Shanghai 201800, P. R. China.

Abstract

Computed Tomography (CT) is an approach that has been extensively applied in many areas of science from understanding structures in living organisms to materials science. In materials science, the study of structures within coatings presents challenges on at least two different levels. First, the structure of the coatings needs to be understood from the atomic scale, where dissolution reactions begin, up to length scales which cover the aggregation of inhibitors and other additives, which take place at ~10^{-5} m, *i.e.* 4 to 5 orders of magnitude. CT is a favourable imaging technique since it allows multiscale information to be obtained non-destructively down to tens of nanometres. In this study X-ray absorption contrast imaging has been used to examine structures created using strontium chromate ($SrCrO_4$) particles embedded in an epoxy film. It has been found that $SrCrO_4$ particles can form clusters that extend a few hundred microns in the plane of the film, span the thickness of the film and have fractal characteristics. There are also volumes of low density epoxy of similar sizes and characteristics to the $SrCrO_4$ clusters. The $SrCrO_4$ clusters have a strong influence on the leaching behaviour since the release changes with time. Initially, leaching is controlled by direct dissolution but, as the clusters dissolve, the release is dominated by the fractal dimension of the cluster. The dissolved clusters leave behind voids filled with electrolyte that provide alternative transport pathways for corrosive ions through the polymer. In this paper, the nature of these clusters will be reviewed and the implication for transport properties and electrochemical assessment will be explored.

Keywords: computed tomography, strontium chromate, inhibited primers, Electrochemical Impedance Spectroscopy (EIS).

1.0 Introduction

Recently, the authors reported the presence of clusters of strontium chromate ($SrCrO_4$) particles within an epoxy film which served as a model paint primer[1,2]. It was found that $SrCrO_4$ particles formed intertwined clusters extending laterally in the plane of the film, the largest of which had fractal dimensions around 2.4. The leaching of inhibitor from these clusters was complicated and followed a range of behaviours exemplified by the non-linear accumulation (on a log-log plot) of Cr in the leachate solution where a linear accumulation with a gradient of 0.5 would indicate Fickian diffusion [1, 3-5]. This behaviour was similar to other studies where the accumulation scaled with t^n where *n* could vary from 1.0 to 0.0 with increasing time. Release rates less than $t^{0.5}$ are difficult to explain. Javierre et al. [6] examined a number of configurations for Fickian diffusion models and indicated that they could not explain a behaviour that is less than $t^{0.5}$. Jenkins and Miller observed that leaching kinetics could go from t^1 for direct dissolution through to $t^{0.5}$ for Fickian dominated diffusion to t^0 when the chromate was completely exhausted [7]. However, the observed leaching profiles are more complicated in that *n* can vary significantly in any individual experiment. Tabor and Warszynski [8] found rates from $t^{0.5}$ to $t^{1.5}$ using various based on the Noyes-Whitney model [9] (*i.e.*, the rate of release is proportional to the difference between the actual concentration and the concentration at saturation). Leaching from clusters with fractal structures might provide a better explanation of the leaching behaviour through the following stages: Leaching begins with direct dissolution of inhibitor particles connected to the external electrolyte followed by dissolution from within the cluster which tends to have a leach rate that reflects the fractal nature of the network. Eventually, the chromate in the cluster is exhausted and *n* will approach zero, and leaching will stop.

The clusters themselves are thus important from the perspective of leaching but also for the transport pathways that are created when the $SrCrO_4$ is dissolved. Here the void created by the dissolution of $SrCrO_4$ provides a pathway for transport of electrolyte including corrodents, and corrosion product (e.g. metal cations) from the interface between the metal and the ”cluster void” to the coating/electrolyte interface.

The purpose of this paper is to elaborate on the influence these networks have on corrosion processes and the consequences for electrochemical impedance spectroscopy (EIS) equivalent circuit modelling. The focus therefore is on electrolyte penetration of the $SrCrO_4$ clusters themselves and the fractal void space left after their dissolution, particularly of pathways that connect the external environment to the metal/coating interface. In this sense this paper is a discussion paper rather than a paper presenting a complete body of new research, although new data are presented. To achieve this objective the paper is divided into two parts with the first part providing an overview of a physical model based on the clusters and the implications on transport from a phenomenological perspective and the second part addressing the implications for both corrosion and EIS.

EIS modeling of coatings and their breakdown often considers the construction of equivalent circuits from the perspective of penetrative pathways from the external electrolyte to the metal/coating interface. Obviously, these structures represent heterogeneities in the coatings which are not easy to quantify in three dimensions. Clearly, Computed tomography (CT) provides the 3D structure of the $SrCrO_4$ clusters and the low density epoxy (LDE, described below), which represents a case of lateral heterogeneity in the coating. Heterogeneity in coatings has been of some interest in recent years [10-14]. Heterogeneity might occur vertically or laterally within coatings and it may arise from structural or chemical variations which lead to a change in properties with location in the coating. Discussion on lateral heterogeneity is often framed in the context of penetrating and non-penetrating paths where, for example, H_2O can diffuse down penetrating paths and reach the metal substrate whereas in non-penetrating paths H_2O will simply reside within the coating down to the base of the non-penetrating path itself. Vertical heterogeneity (layering) has been explored to understand the physical processes behind the dispersive behavior associated with the use of constant phase elements (CPE) in EIS equivalent circuit modeling. For example Musiani et al. [11] found that having differences in permittivity and resistivity with depth offered a good explanation for the need for a CPE element. This is an example of heterogeneous *property* distributions. In the case presented here we describe *structural* heterogeneity caused by the clustering of $SrCrO_4$ particles because of their

encapsulation in the epoxy matrix of an inhibited primer. We have classified this as *structural* heterogeneity because the density of $SrCrO_4$ particles across the coating is fairly constant but it is the cluster structure that is causing the heterogeneity. Similarly the LDE is an example of *structural* heterogeneity since the LDE is well distributed over the sample but there are penetrative volumes of LDE indicating heterogeneity within these structures.

2.0 Experimental

2.1 Materials and Sample Preparation

This area has been covered in previous studies and will only be briefly addressed here[1,15]. Epikote® 828 (Resolution Performance Product) is a medium viscosity liquid epoxy resin produced from bisphenol A and epichlorohydrin. Hardener 92133 was supplied by Akzo Nobel Aerospace Coating (ANAC). $SrCrO_4$ was obtained from Akzo-Nobel ANAC [16]. Samples were prepared by adding $SrCrO_4$ (0.5 g) to the Epikote (1 g) followed by hardener 92133 (2.2 ml), allowing the mixture to stand (5 - 10 minutes) at room temperature and then coated onto glass microscope slides, resulting in an approximately 100 μm thick film. Films were left to dry overnight at room temperature and then cured at 40°C for 7 days. A slither of the coating was removed from this film for tomographic analysis. For the leaching experiment, samples were immersed in the 0.1 M NaCl solution, prepared from analytical reagents, for 20 minutes at room temperature. The sample was then allowed to dry prior to X-ray CT examination.

2.2 X-ray CT Studies

The X-ray CT studies have also been described before [1]. Briefly, the X-ray CT projection images were acquired at room temperature and ambient pressure at the Shanghai Synchrotron Radiation Facility (SSRF) BL13W imaging beam-line. Projection images were collected at 15.5 keV, with an acquisition time of 2 seconds for each projection. A total of 900 projection images was collected with a total sample rotation angle of 180°.

CT slices were reconstructed from the projection images. First, background corrections were applied using flat-field and dark-current images. Normalized images were subject to Paganin's phase-retrieval, with parameters tuned to optimize the signal-to-noise ratio and to minimize the edge enhancement without loss of resolution [17]. Finally, the slices were reconstructed by using the method of filtered back-projection of the parallel X-ray beam [17]. Any ring artefacts in the slices arising from the reconstruction were subsequently corrected [18]. The reconstructed CT datasets prior and subsequent to electrolyte exposure were aligned by translation and rotation of slices to maximise the cross-correlations between corresponding images. These processed datasets, containing information of absorption indices, that were used for further analysis by using the data constrained modeling (DCM) method [19,20], in which the constituent material phases were spatially resolved using an optimized least squares minimization approach [19].

3.0 Results and Discussion

As described in the introduction, this paper is divided into two parts. In the first part an overview of recent CT studies is provided. In the second part this overview extends the discussion of these CT results for transport within the inhibited primers, corrosion and finally implications for EIS modeling. Figure 1 present a visual summary of the results obtained from previous studies. In this figure different components are represented by different colours, with the $SrCrO_4$ particles in red, and the two largest $SrCrO_4$ particles in orange and yellow (2nd largest), normal epoxy in grey-blue and the LDE in dark blue (Figure 1(a), (b) and (c).) The largest cluster, which is isolated as the blue cluster in the inset in Figure 1(c), spans the width of the epoxy film.

3.1 Overview of recent CT studies

3.1.1 Polymer Matrix

Ideally a discussion of the polymer matrix should begin with the pure polymer, however, preliminary studies performed in our laboratories on the pure polymer indicate that the internal structures observed using CT on inhibited primers were not evident in the pure polymer indicating that the structures within the polymer itself are associated

with the presence of the second phase. Consequently, this discussion will begin with the polymer matrix in the presence of other phases.

Several scenarios can arise with the structural relationship the additives (fillers, inhibitors, UV absorbers….) have with each other as well as to the polymer matrix which have important implications for the transport of species within the paint system. In determining transport pathways through these systems it is important to know whether the inhibitor can diffuse through the polymer or not. This will depend on both the nature of the inhibitor as well as the polymer matrix. The larger the inhibitor molecule then the less likely it will be able to diffuse through the polymer matrix. At the atomic level the polymer matrix has porosity between the polymer chains called the molecular pore volume which can be probed directly using positron techniques [21-23]. For the epoxies used in this study it was 5.5 Å and of a similar size to the hydrated chromate ion (CrO_4^{2-}) at ~ 5 Å. Other epoxies have been reported to have even smaller molecular pore volumes (see Table 1). In situations where the inhibitor size is similar to or smaller than the molecular pore volume of the polymer then it ends up being encapsulated in the paint system unless it is either connected to the external electrolyte via a defect larger than the molecular pore volume which intersects the $SrCrO_4$ clusters or it is already at the external surface and exposed to the electrolyte as a result of the manufacture of the coating (Figure 1(a) and (b)). Where it is exposed to the external electrolyte then the "encapsulation" provided by the polymer is lost since the inhibitor can be directly dissolved into solution. Table 1 presents some typical inhibitor sizes and molecular pore volumes for polymer systems. The data for the inorganic oxyanions are for the mono-nuclear species, polynuclear species will be larger. The figures do not include waters of hydration which will make the ion and its hydration sphere larger. For both inorganics and organics it is also not clear whether the hydration sphere moves with the ion or whether there is a series of water exchange steps involving sequential hydrogen bond breaking and formation with different water molecules. This type of transport for waters of hydration has been discussed in the context of amphiphiles [24].

A second type of connected volume within the epoxy which was observed using X-ray CT is associated with areas of different epoxy density (Figure 1). This is a little studied and potentially controversial area still under investigation by the authors. X-ray

absorption contrast is one of the few techniques that can be used to detect differences in polymer density and there is no doubt that there are different absorption contrasts within the polymer reflecting different densities within many epoxies studied by the authors, but the exact nature of the differences is still under investigation. An example of a slice through a $SrCrO_4$ inhibited epoxy shows the X-ray absorption density contrast associated with the epoxy, $SrCrO_4$ particles (bright particles) and a lower density (darker) than the epoxy itself (Figure 2). Although it is clear that the lower absorption contrast region is associated with a lower density in the polymer density, it may not be straightforward to associate it with specific properties such as crosslink density. Part of the problem here is related to having only an incomplete knowledge of all the ingredients of the epoxy including surfactants (which may include Si in silanes), flow agents such as SiO_2 and catalysts (which may include chlorine containing compounds or transition metals such as Ru in the Grubb's catalyst used in self healing studies of epoxies [25,25]). Small amounts of Si, Cl or Ru can significantly change the absorption contrast hence the difficulty in interpreting changes in epoxy absorption density as changes in cross link density. On the other hand local variations in the distribution of these additives means that their distribution can, in principle, be studied. Even if the LDE regions are related to cross linking density it is not clear whether they are regions of high or lower crosslink density. It could be argued that regions of high cross-linking density may provide a more rigid but open network through which water can migrate since in regions where there is less cross linking, the polymer segments are not held rigidly in place by the cross-linking agent and can collapse on themselves thus closing any pathways and increasing the local density. If these regions eventually open up with water uptake and swelling then the X-ray contrast may switch, and what was formerly high density, might become low density.

Previously the authors have found no evidence that the LDE volumes provided alternative transport pathways for the inhibitor over the timescales studied (7 days immersion in 0.1M NaCl solution). However, they may provide pathways for H_2O to freely penetrate the film. Based on their size alone small ions (e.g. Cl^- and OH^- and cations), could also freely penetrate the film, but because of their charge and the need

for charge neutrality it may imply that ion transport proceed via an exchange process which will be slower than water diffusion.

3.1.2 Structures formed by particle clusters

In instances where the molecular pore volume is small the epoxy will act as an encapsulating system and the structure of the distributed $SrCrO_4$ particles will dominate the transport of the inhibitor. In these circumstances transport of the inhibitor will be dictated by the geometry of the inhibitor particle distribution. Generally, formulators require good dispersion of all phases, however, until now it has not been clear what constitutes "good dispersion". This topic is often also couched in terms of the pigment volume concentration (PVC) where, if the amount of solids is above the critical pigment volume concentration (CPVC), then there may not be sufficient polymer to completely coat the inhibitor particles. It appears possible to disperse the $SrCrO_4$ particles into different configurations from extended clusters whose volume is described by fractal dimensions less than 3 to isolated clusters that effectively have a fractal dimension of 3 [27]. For dispersed clusters overall leaching will be the sum of leaching characteristics of the individual clusters that are connected to the external electrolyte. The largest clusters have the lowest fractal dimensions and the smaller clusters approach a fractal dimension of 3, hence the leaching profile will be complicated. Some of these clusters will extend from the external surface to the metal/film interface where they will encounter a range of possible surface conditions. For example, the surface of the metal may have a surface oxide or a near surface deformed layer if untreated after polishing or abrading [28-33], or an anodized [28] or conversion coated surface [28,34] if treated.

In the paint film, the development of transport pathways within clusters via the dissolution of $SrCrO_4$ is not likely to be as straightforward as a dissolution front moving through the $SrCrO_4$ clusters. As can be seen in Figure 3(a) before an epoxy containing $SrCrO_4$ particles is exposed to an electrolyte there may already be a network of pores that penetrate through the cluster of $SrCrO_4$ particles simply because the particles themselves are fragmented and cracked (effectively the local PVC>CPVC). This possibility has previously been reported by Foyet et al. [35]. In the case presented here the cracks are one to two hundred nanometres wide and many microns long (Figure 3). These paths could provide a route for the rapid uptake of water and the initiation of

$SrCrO_4$ dissolution. It is not clear whether diffusion through these types of networks would be faster than diffusion through the epoxy itself given that the cracks may be filled with concentrated solution or gels resulting from the dissolution of the $SrCrO_4$ particles. Water transport has been shown to slow by up to an order of magnitude in amphiphiles due to confinement of water. Concentrated gels at the chromate particle surfaces may also have a similar effect on the kinetics of water, since all the chromate ion itself is known to slow by as much as an order of magnitude in concentrated solutions [36].

The dissolution of the $SrCrO_4$ particles within the clusters is evident in Figure 1(e) and (f) where the largest cluster of $SrCrO_4$ particles is broken into smaller clusters by the dissolution of a bridge which joins two parts of the cluster, but some $SrCrO_4$ particles remain, so complete dissolution has not been achieved after this immersion time. The dissolution the $SrCrO_4$ particles is also evident in the scanning electron micrograph in Figure 3. Clearly, after a period of immersion, the remaining $SrCrO_4$ particles have rounded edges creating a void space around them. Presumably this is due to dissolution from the surface of the particle while void spaces apparent in the SEM might have been filled with gel or electrolyte which was removed during polishing for sample preparation. It should be noted that while we have reported on the fractal dimension of individual clusters, the fractal dimension of the network of void space surrounding the clusters of $SrCrO_4$ particles if connected (c.f.Figure 3) would be even lower than the largest clusters, *i.e.,* less than approximately 2.4, but it will approach the fractal dimension of the cluster as complete dissolution of the $SrCrO_4$ particles is approached.

To this point we have only examined one inorganic additive, however, real paints have a number of inorganic and organic additives. These additional additives may lead to other secondary networks within the paint coating that need consideration. As reported by Lee et al. [37], additives may act as sources and sinks within porous networks. In this case the initial source of the inhibitor are the $SrCrO_4$ clusters, however other phases may act as sinks if they reversibly or irreversibly adsorb chromate. Moreover, given the fractal nature of some of the structures observed with the $SrCrO_4$ particles, it is feasible that the inhibitor could be "lost" down pathways where the diffusion length to the external surface is exceedingly long.

Other effects might also be achieved with additives. In our work we have observed that soluble $CaSO_4$ may provide alternative transport pathways for the leaching of inhibitors [37]. For example a defect made at the site of a $CaSO_4$ particle (Figure 4) in an epoxy containing $SrCrO_4$ and $CaSO_4$ not only resulted in the dissolution of the $CaSO_4$ particle itself but appeared to facilitate the dissolution of surrounding $SrCrO_4$ particles suggesting connecting pathways between the two phases. Importantly, the implications of these studies are only beginning to be explored.

3.2 Transport and Corrosion

In this section the potential role that the heterogeneity introduced by the $SrCrO_4$ clusters and other structures may have in the development of corrosion is examined. Heterogeneous structures in paint coatings have been of interest for a number of years [6,710,11,15,16,38,41]. Heterogeneity within coatings can occur vertically, such as with layering or gradients (Figure 5(a) and (b)) or laterally such as with preferred, penetrative paths (Figure 5(b) to (d)) [22]. Layering might arise from changes in either the *structure* or the *properties* of the coating. In the former case different structures or compositions in different layers of the coating will lead to concentration gradients from a materials perspective. Alternatively, there may be property gradients such as changes in resistivity with depth through the coating which also cause heterogeneity in coatings and lead to dispersion effects explaining the need for constant phase elements to replace capacitances in equivalent circuits [10,13,42]. (Of course, ultimately, property gradients result from the change in material as a function of depth.) Most importantly, gradients within heterogeneous pathways are likely to occur as part of the corrosion process, particularly if the migrating species are confined to the pathways and are unable to diffuse through the epoxy. These gradients will result from the gradual release of inhibitor at the pore/electrolyte interface or the buildup of corrodent species at the metal/pore base. An example of heterogeneity within a $SrCrO_4$ cluster is shown in Figure 1(e) where $SrCrO_4$ remains in a void created by the partial dissolution of a cluster.

The species of interest migrating through the heterogeneous pathways include H_2O, O_2, OH^-, inhibitor ions, metal ions and counterions. Penetrative heterogeneous structures,

such as the $SrCrO_4$ clusters, the voids that remain after dissolution of the $SrCrO_4$ clusters and the LDE, potentially have a role to play in the transport of all of these species during the activation and corrosion processes. Generally, water uptake is rapid upon exposure of inhibited coatings to an electrolyte [35,41,43,44] as was the case for the epoxy film presented here which was saturated in less than four hours [43,45]. The uptake is not so fast in the pure polymer where better barrier properties are developed and H_2O penetration may take many days [35,41,42]. Water uptake in epoxy is reported to be faster than that of anions such chloride ions [43,45]. The H_2O uptake is thought to occur via diffusion of water through the polymer matrix, however, it is possible that other structures may play a role such as penetrative pores reported for electrodeposited epoxys without inhibitors [41,46,47]. In the samples studied here, where the inhibitor is present, there may be accelerated H_2O transport through the LDE components. Alternatively, if there are $SrCrO_4$ clusters connected to the external surface, then migration of water through the cluster along defect pathways in the $SrCrO_4$ particles is also possible (Figure 5(c)). Whether migration through the cluster is a faster process than through the polymer matrix in this very early stage of water uptake is not known, although faster H_2O penetration through inhibited primers compared to the parent pure epoxy suggests that "short-circuit" pathways are present when the inhibitor is present [35]. Setting aside the question of migration rates, there appears to be five types of penetrative pore networks that may be important for the transport of species including:

i. through the polymer itself at very small scales typical of the molecular pore volume,
ii. through additive clusters (e.g. $SrCrO_4$) that connect the external electrolyte to the metal/film interface,
iii. associated with either PVCs that are locally higher than the CPVC or PVCs that are globally higher than the CPVC. These are distinguished from those in (ii) because they are related in interparticle void due to lack of polymer rather than void created by the dissolution of the particle,
iv. Local variation in density of the polymer itself such as with the LDE components mentioned above,
v. Mixed pore networks particularly those that are not connected to the external surface but reach the metal/coating interface or vice versa

Summarising with respect toFigure 5, the types of pore networks mentioned in the literature have a range of scales from that of molecular pore volume (case (i)) to micro-porous defects (case (ii)). For example, penetrative pathways through the polymer itself may range in scale from micropores [41] or domains with different polymer density (LDE) [1,2] down to pathways through the intramolecular volume [22, 35]. There is also likely to be a strong dependence on the chemistry of the polymer and the cross linking agent [22, 23].

In the case where there are additives, then additional pathways might be introduced forming channels through the additive network creating heterogeneous penetration (case (iii)-(v), Figure 5(c)). In this case, there are several possibilities related to different aspects of the coating. One crucial aspect is the PVC; if it is higher than the CPVC then there will not be sufficient polymer to coat all the pigment resulting in voids in the coatings (case (iii), Figure 5(b)) [48]. This can also occur locally when the pigment is not mixed thoroughly with the polymer creating regions where the *local* PVC > CPVC (Figure 5(b) red ellipse). The addition of more than one additive phase further complicates the picture with the potential introduction of more networks as well as sinks for inhibitors [37].

3.3 Electrochemistry

The nature of electrochemical impedance spectroscopy (EIS) means that the penetrative pore networks, which provide conduction through the coating, will dominate the EIS measurements [41]. Thus from an EIS perspective, reactions that occur within the pores and at the base of the pores are of critical importance. The simplified Randles circuit is generally accepted as a good equivalent circuit model for a coating without exposure to an electrolyte (Figure 6(a)). However, this circuit very quickly evolves into more complicated and often controversial model circuits when a coating is exposed to an electrolyte. This initial response of the coating on exposure to electrolyte (often referred to as activation) is generally modeled in EIS using the equivalent circuit described in Figure 6(b). It includes a coating capacitance (C_c) and pore network resistance (R_c) for the coating and a double layer capacitance (C_{dl}) and charge transfer resistance (R_{ct}) for the coating/metal interface. After the initial penetration of water throughout the coating, corrodent migration results in the appearance of other active

species at the metal/coating interface at the base of the penetrative pores. At this stage the process of underfilm corrosion and delamination begins. The equivalent circuit that is often used here includes additional CPE elements in series with the pore resistance or the nature of this electrode may require a Warburg impedance to explain diffusion control across the interface. Phase angle information is often useful for determining which elements to use [49].

Often CPE elements are used to replace the pure capacitors in the equivalent circuits presented in Figure 6 to produce better fits. The justification for the use of CPE elements may have several origins based on differences in properties within the coating that lead to dispersive behaviours as discussed above. While the $SrCrO_4$ clusters and other pore networks reported here do not change our understanding of the nature of the corrosion and passivation reactions at the metal/coating interface, they will influence the transport of reactants to and from the active sites at the coating/metal interface and will have different pore properties to each other as well as gradients or layers within pore networks as discussed below.

The tomography work here indicates that there is likely to be heterogeneous penetration along the $SrCrO_4$ pore networks, as well as possible homogenous or heterogeneous (through the LDE) penetration of H_2O, meaning that there will be individual equivalent circuits for all these different types of pathways and the impedance response will be the sum of these pathways (assuming they are independent), but dominated by those pores that have the highest ionic conduction [41,50]. A summary of these circuits is presented in Figure 7.

Generally, within the pore networks, there will be ongoing changes in concentration of a range of species, specifically inhibitors, corrodents, and reaction products. The presence of inhibitors and reaction products will influence the transport of O_2 and corrodents to the base of penetrative pores where the corrosion reactions occur by acting as diffusion barriers. In the longer term, reaction products are likely to eventually block the pores. In Figure 7, the interface has not been treated in detail with just the impedance Z_{int} assigned to it.

Focusing first on the LDE pore networks (Figure 7, top) and $SrCrO_4$ clusters (Figure 7, 2nd from top), it is likely that there will be concentration gradients within these networks, justifying the use of a CPE for each equivalent circuit. In the case of the LDE, differential H_2O penetration from the mouth(s) of the pore network to the coating/metal interface will occur initially, oxygen concentrations will also vary and electrolyte concentration gradients might also potentially develop. For the $SrCrO_4$ clusters differential dissolution along the cluster from their mouth(s) to the coating/metal interface means that the properties within the dissolving cluster will vary from point to point and with time. Moreover, the fractal nature of the cluster may mean that there are pockets of chromate concentrations within the cluster and the chromate distribution will not even follow a monotonic gradient through the pore network. This is because the dissolution front does not move smoothly through the cluster and so the $SrCrO_4$ particles are not instantaneously replaced by electrolyte. Indeed a shrinking core model [7, 51-53], representing dissolution of the particle from the outside inward, will apply to every particle in the clusters. In fact, the concentration profiles of the pore networks through the partially dissolved $SrCrO_4$ clusters may be quite complicated with eventual penetration of electrolyte into the pore network: concentrated chromate solution means chloride and sodium ions will need to undergo an ion exchange process to maintain local charge neutrality in order to penetrate the electrolyte within the pore network left by dissolved $SrCrO_4$.

There may also be mixed networks such as presented in Figure 7 (3rd from top), where a cluster connected to the coating/metal interface is penetrated by H_2O that has diffused from the electrolyte interface through the epoxy. This pathway will contain components from both the epoxy matrix as well as the clusters, hence, the use of two components (R_P, R_{P2}, CPE_{C1}, CPE_{C2}) in series. While this model can be reduced to a single resistance ($R = R_P + R_{P2}$) and CPE element ($CPE = CPE_{C1} + CPE_{C2}$), they are separated for the purposes of illustration here. The use of CPE elements for both these components is justified on the basis of heterogeneous penetration of H_2O through the epoxy and concentration gradients within the $SrCrO_4$ component as described above for the penetrative $SrCrO_4$ clusters. At the bottom of Figure 7 is the equivalent circuit for

the epoxy itself. As with other polymers, CPE elements would be justified on the basis of heterogeneous penetration pathways for H_2O or properties through the coating.

It is also worth noting that while the interface has been treated similarly in the equivalent circuits in Figure 7, (Z_{INT}), the types of reaction that occur at the metal/film interface at the base of the penetrative pore networks will be different between pore networks depending on whether chromate is present or not. Ironically, the initial penetration of H_2O and dissolution of an amount of $SrCrO_4$ below the critical inhibitor concentration (~ 10^{-5}M) [54,55] may mean that initially the most active short circuit pathways through the film are those through the chromate channels since chromate will act as an oxidizing agent. At longer times, when more $SrCrO_4$ is dissolved passivation will occur [54]. In the case where there is no chromate, the delivery of water (and oxygen) to the interface will facilitate oxidation reactions causing some interim passivation, but these may be incipient sites for further corrosion once corrosive ions appear. So, initially at least, at the base of those penetration paths, Z_{INT} will have at least two general equivalent circuits: comprising one for the penetration channels associated with the $SrCrO_4$ and the other for water penetration channels.

At longer times, when the corrosion reactions occur at base of the penetrating pore networks then metal ions will be generated, which migrate away from the active site into the network and may form precipitates within the network where the electrolyte is not as acidic as at the anodic corrosion site. This precipitate will act as a diffusion barrier to corrodents changing the kinetics at the active corrosion site. These sites may eventually form the larger defects that are observed in coatings in addition to other sites where defects through the paint coating occur.

Finally, the equivalent circuit models depicted in Figure 7 are assumed to be independent of each other based on the fact that all the electrochemistry occurs at the base of the pore network and presumably the transport through the pore network is significantly faster than through the polymer. Penetration of conducting electrolyte into the polymer network may eventually lead to reaction on the pore walls, which will further complicate analysis and may require a transmission line approach.

4.0 Conclusions

In the paper we have described some recent advances in the understanding of the internal structure and distribution of inhibited primers. Specifically we have found that $SrCrO_4$ particles can form extended clusters within primers which have fractal dimensions. Additionally, there appear to be regions of LDE that extend through the coating. Both these features are likely to be transport paths within the coating and form the heterogeneous structures often referred to in EIS studies which can lead to dispersion effects. In the case of the void network formed during the dissolution of the $SrCrO_4$ clusters then concentration gradients are likely to form from the mouth(s) of the cluster to the coating metal interface (chromate cannot diffuse through the polymer in this system). For the LDE there will be water gradients through the coating during activation, but at latter times there may also be electrolyte gradients. A number of equivalent circuits models have been proposed for different heterogeneous pathways.

Acknowledgements: GET, PDL and JC would like to thank the EPSRC for funding the LATEST 2 programme grant, and partly the Research Complex at Harwell (EP/102249X/1).

5.0 References

1 A. E. Hughes, A. Trinchi, F. F. Chen, Y. S. Yang, I. S. Cole, S. Sellaiyan, J. Carr, P. D. Lee, G. E. Thompson and T. Q. Xiao,Revelation of Intertwining Organic and Inorganic Fractal Structures in Polymer Coatings, Advanced Materials, (2014), n/a-n/a.

2 A. E. Hughes, A. Trinchi, F. F. Chen, Y. S. Yang, I. S. Cole, S. Sellaiyan, J. Carr, P. D. Lee, G. E. Thompson and T. Q. Xiao,The Application of Multiscale Quasi 4d Ct to the Study of Srcro4 Distributions and the Development of Porous Networks in Epoxy-Based Primer Coatings, Progress in Organic Coatings, 77, (2014), 1946-56.

3 A. E. Hughes, Cole, I.S., Muster, T.M. and Varley, R.J.,Combining Green and Self Healing for a New Generation of Coatings for Metal Protection, Nature Asia Materials, 2, (2010), 143-51.

4 A. Nazarov, D. Thierry, T. Prosek and N. Le Bozec,Protective Action of Vanadate at Defected Areas of Organic Coatings on Zinc, Journal of the Electrochemical Society, 152, (2005), B220-B7.

5 T. Prosek and D. Thierry,A Model for the Release of Chromate from Organic Coatings, Progress in Organic Coatings, 49, (2004), 209-17.

6 E. Javierre, S. J. García, J. M. C. Mol, F. J. Vermolen, C. Vuik and S. Van Der Zwaag,Tailoring the Release of Encapsulated Corrosion Inhibitors from Damaged Coatings: Controlled Release Kinetics by Overlapping Diffusion Fronts, Progress in Organic Coatings, 75, (2012), 20-7.

7 D. R. Jenkins and A. D. Miller, A Model of Chromate Leaching from Inhibited Primers, (2009).

8 Z. Tabor and P. Warszyński,Modeling Dissolution Controlled Release of Inhibitor from a Damaged Coating, Corrosion Science, 82, (2014), 290-6.

9 A. A. Noyes and W. R. Whitney,The Rate of Solution of Solid Substances in Their Own Solutions, The Journal of the American Chemical Society, 19, (1897), 930-4.

10 S. Amand, M. Musiani, M. E. Orazem, N. Pébère, B. Tribollet and V. Vivier,Constant-Phase-Element Behavior Caused by Inhomogeneous Water Uptake in Anti-Corrosion Coatings, Electrochimica Acta, 87, (2013), 693-700.

11 M. Musiani, M. E. Orazem, N. Pébère, B. Tribollet and V. Vivier,Constant-Phase-Element Behavior Caused by Coupled Resistivity and Permittivity Distributions in Films, Journal of the Electrochemical Society, 158, (2011), C424-C8.

12 B. Hirschorn, M. E. Orazem, B. Tribollet, V. Vivier, I. Frateur and M. Musiani,Constant-Phase-Element Behavior Caused by Resistivity Distributions in Films: Ii. Applications, Journal of the Electrochemical Society, 157, (2010), C452-C7.

13 B. Hirschorn, M. E. Orazem, B. Tribollet, V. Vivier, I. Frateur and M. Musiani,Constant-Phase-Element Behavior Caused by Resistivity Distributions in Films: I. Theory, Journal of the Electrochemical Society, 157, (2010), C458-C63.

14 A. Trueman, S. Knight, J. Colwell, T. Hashimoto, E. Koroleva and G. Thompson, Micro-Structural Characterisation of Paint Using Ultra-Microtome Sem, (2012).

15 H. Selvakumar Sellaiyan, A.E., Smith, S.V., Unedono, A., Sullivan, J., Buckman, S.,Leaching Properties of Chromate-Based Epoxy Matrix Using Radiotracer, Pals and Sem, (2013),

16 S. Sellaiyan, A. E. Hughes, S. V. Smith, A. Uedono, J. Sullivan and S. Buckman,Leaching Properties of Chromate-Containing Epoxy Films Using Radiotracers, Pals and Sem, Progress in Organic Coatings, 77, (2014), 257-67.

17 D. Paganin, Mayo, S.C., Gureyev, T.E., Miller, P.R. & Wilkins, S.W.,Simultaneous Phase and Amplitude Extraction from a Single Defocused Image of a Homogeneous Object, Journal of Microscopy - Oxford, 206, (2002), 33 - 40.

18 T. E. Gureyev, Nesterets, Y., Ternovski, D., Thompson, D., Wilkins, S.W., Stevenson, A.W., Sakellariou A. andTaylor, J.A., (2011).

19 S. yang, Gureyev T.E., Tulloh, M.B., Clennell, M.B., Pervukhina, M.,Feasibility of a Data Constrained Prediction of Hydrocarbon Reservoir Sandstone Microstructures, Measurement Science & Technology, 21, (2010),

20 S. Yang, Tulloh, A., Chu, C. Chen, F., https://data.csiro.au/dap/landingpage?pid=csiro:9448.

21 M. M. Madani, R. R. Miron, R. D. Granata and S. P. E. S. P. E. Soc Plast Engineers, Interfacial Free Volume Measurements of Epoxy on Aluminum by Pals, (1999).

22 M. M. Madani, H. L. Vedage and R. D. Granata,Evaluation of Polyimide Coatings Integrity by Positron Annihilation Lifetime Spectroscopy and Electrochemical Impedance Spectroscopy, Journal of the Electrochemical Society, 144, (1997), 3293-8.

23 M. M. Madani, R. R. Miron and R. D. Granata,Pals Free Volume Study of Dry and Water Saturated Epoxies, Journal of Coatings Technology, 69, (1997), 45-&.
24 G. Stirnemann, F. Sterpone and D. Laage,Dynamics of Water in Concentrated Solutions of Amphiphiles: Key Roles of Local Structure and Aggregation, Journal of Physical Chemistry B, 115, (2011), 3254-62.
25 D. Y. Wu, S. Meure and D. Solomon,Self-Healing Polymeric Materials: A Review of Recent Developments, Progress in Polymer Science, 33, (2008), 479-522.
26 J. D. Rule, N. R. Sottos and S. R. White,Effect of Microcapsule Size on the Performance of Self-Healing Polymers, Polymer, 48, (2007), 3520-9.
27 S. Yang, Trinchi, A. Hardin, S.G. Hughes, A.E.,To Be Published, AIMS's Journal, (2015),
28 T. H. Muster, Hughes, A.E., Thompson. G.E., Cu Distributions in Aluminium Alloys, Nova Science Publishers, New York, (2009).
29 M. Fishkis and J. C. Lin,Formation and Evolution of a Subsurface Layer in a Metalworking Process, Wear, 206, (1997), 156-70.
30 H. Leth-Olsen, J. H. Nordlien and K. Nisancioglu,Filiform Corrosion of Aluminium Sheet. Iii. Microstructure of Reactive Surfaces, Corrosion Science, 40, (1998), 2051-63.
31 A. Afseth, J. H. Nordlien, G. M. Scamans and K. Nisancioglu,Effect of Heat Treatment on Filiform Corrosion of Aluminium Alloy Aa3005, Corrosion Science, 43, (2001), 2093-109.
32 Z. Zhao and G. S. Frankel,Surface Layer Dissolution Kinetics of Aluminum Alloy 7075 in Various Tempers, Corrosion, 63, (2007), 613-24.
33 Z. Zhao and G. S. Frankel,On the First Breakdown in Aa7075-T6, Corrosion Science, 49, (2007), 3064-88.
34 R. G. Buchheit, Hughes, A.E., Chromate and Chromate-Free Coatings, ASM International, Mterials Park, Oh, USA, (2003).
35 A. Foyet, T. H. Wu, A. Kodentsov, L. G. J. van der Ven, G. de With and R. A. T. M. van Benthem,Absorption of Water and Corrosion Performance of a Clear and Pigmented Epoxy Coating on Al-2024 Alloy, Coatings for Corrosion Protection, 25, (2010), 31-9.
36 M. Ball and G. Oldham,Diffusion Coefficients of the Chromate Ion in Concentrated Solutions, Journal of the Chemical Society (Resumed), (1963), 3472-4.
37 S. B. Lee and S. Torquato,Porosity for the Penetrable-Concentric-Shell Model of 2-Phase Disordered Media - Computer-Simulation Results, Journal of Chemical Physics, 89, (1988), 3258-63.
38 B. R. Hinderliter, S. G. Croll, D. E. Tallman, Q. Su and G. P. Bierwagen,Interpretation of Eis Data from Accelerated Exposure of Coated Metals Based on Modeling of Coating Physical Properties, Electrochimica Acta, 51, (2006), 4505-15.
39 R. S. Fishman, D. A. Kurtze and G. P. Bierwagen,Pigment Inhomogeneity and Void Formation in Organic Coatings, Progress in Organic Coatings, 21, (1993), 387-403.
40 J. Kittel, N. Celati, M. Keddam and H. Takenouti,Influence of the Coating–Substrate Interactions on the Corrosion Protection: Characterisation by Impedance Spectroscopy of the Inner and Outer Parts of a Coating, Progress in Organic Coatings, 46, (2003), 135-47.
41 V. B. Mišković-stanković, D. M. Dražić and M. J. Teodorović,Electrolyte Penetration through Epoxy Coatings Electrodeposited on Steel, Corrosion Science, 37, (1995), 241-52.
42 I. M. Zin, R. L. Howard, S. J. Badger, J. D. Scantlebury and S. B. Lyon,The Mode of Action of Chromate Inhibitor in Epoxy Primer on Galvanized Steel, Progress in Organic Coatings, 33, (1998), 203-10.
43 J. M. Hu, J. Q. Zhang and C. N. Cao,Determination of Water Uptake and Diffusion of Cl- Ion in Epoxy Primer on Aluminum Alloys in Nacl Solution by Electrochemical Impedance Spectroscopy, Progress in Organic Coatings, 46, (2003), 273-9.
44 M. Santa, R. Posner and G. Grundmeier,Wet- and Corrosive De-Adhesion Processes of Water-Borne Epoxy Film Coated Steel: Ii. The Influence of Γ -Glycidoxypropyltrimethoxysilane as an Adhesion Promoting Additive, Journal of the Electrochemical Society, 158, (2011), C36-C41.
45 J. Mardel, S. J. Garcia, P. A. Corrigan, T. Markley, A. E. Hughes, T. H. Muster, D. Lau, T. G. Harvey, A. M. Glenn, P. A. White, S. G. Hardin, C. Luo, X. Zhou, G. E. Thompson and J. M. C. Mol,The Characterisation and Performance of Ce(Dbp)(3)-Inhibited Epoxy Coatings, Progress in Organic Coatings, 70, (2011), 91-101.
46 V. B. Miskovic-Stankovic, Z. Z. Ž Lazarević, Z. Kačarević-Popović and D. M. Dražić,Corrosion Behaviour of Epoxy Coatings on Modified Aluminium Surfaces, Bulletin of Electrochemistry, 18, (2002), 343-8.

47 V. B. Mišković-Stanković, M. R. Stanić and D. M. Dražić,Corrosion Protection of Aluminium by a Cataphoretic Epoxy Coating, Progress in Organic Coatings, 36, (1999), 53-63.
48 G. Bierwagen, R. Fishman, T. Storsved and J. Johnson,Recent Studies of Particle Packing in Organic Coatings, Progress in Organic Coatings, 35, (1999), 1-9.
49 F. Mansfeld, M. W. Kendig and S. Tsai,Evaluation of Corrosion Behavior of Coated Metals with Ac Impedance Measurements, Corrosion, 38, (1982), 478-85.
50 M. W. Kendig and H. Leidheiser Jr,Electrical Properties of Protective Polymer Coatings as Related to Corrosion of the Substrate, Journal of the Electrochemical Society, 23, (1976), 982-9.
51 S. A. Furman, F. H. Scholes, A. E. Hughes and D. Lau,Chromate Leaching from Inhibited Primers - Part Ii: Modelling of Leaching, Progress in Organic Coatings, 56, (2006), 33-8.
52 J. Y. Kim, C. L. Kim and C. H. Chung,Modeling of Nuclide Release from Low-Level Radioactive Paraffin Waste: A Comparison of Simulated and Real Waste, Journal of Hazardous Materials, 94, (2002), 161-78.
53 J. Y. Kim, C. L. Kim and C. H. Chung,Modeling of Nuclide Releases from Perforated Radioactive Paraffin Waste Containers, Journal of Nuclear Materials, 303, (2002), 92-8.
54 M. W. Kendig and R. G. Buchheit,Corrosion Inhibition of Aluminum and Aluminum Alloys by Soluble Chromates, Chromate Coatings, and Chromate-Free Coatings, Corrosion, 59, (2003), 379-400.
55 A. R. Trueman,Determining the Probability of Stable Pit Initiation on Aluminium Alloys Using Potentiostatic Electrochemical Measurements, Corrosion Science, 47, (2005), 2240-56.
56 C. E. Housecroft, Sharpe, A.G., Inorganic Chemistry, Pearson Eduucation Ltd, Harlow, (2012).
57 H. Hart, Schuetz, R.D., Organic Chemistry, Houghton Mifflin Company, Boston, (1972).
58 K. D. Ralston, S. Chrisanti, T. L. Young and R. G. Buchheit,Corrosion Inhibition of Aluminum Alloy 2024-T3 by Aqueous Vanadium Species, Journal of the Electrochemical Society, 155, (2008), C350-C9.
59 Y. Dong and Q. Zhou,Relationship between Ion Transport and the Failure Behavior of Epoxy Resin Coatings, Corrosion Science, 78, (2014), 22-8.
60 B. P. Ho, H. J. Chul, M. L. Young, A. J. Hill, S. J. Pas, S. T. Mudie, E. Van Wagner, B. D. Freeman and D. J. Cookson,Polymers with Cavities Tuned for Fast Selective Transport of Small Molecules and Ions, Science, 318, (2007), 254-8.

Figure Captions

Figure 1: Microstructures of an epoxy primer containing $SrCrO_4$ particles. (a) 3D distribution of all components of the epoxy including epoxy (grey-blue), low density epoxy (LDE in blue) and $SrCrO_4$ particles (red), largest $SrCrO_4$ cluster (orange) and second largest $SrCrO_4$ cluster (yellow). Light blue arrows indicate where the largest cluster intersects the external surface of the paint. (b) As for (a) except the epoxy and LDE have been removed. Green ellipse indicates the region of arrows in (a), and light blue rectangle indicates the magnified region (c). In (c) the green arrows indicate a selection of points where the LDE intersects the external surface as well as internally. The inset in (c) shows the five largest clusters with the largest in blue and indicates the width of the epoxy film. (d) Shows a bridge between two regions of the largest $SrCrO_4$ cluster (blue) amid other clusters and (e) shows the same region where the bridge has been dissolved, but indicating that some particles still remain.

Figure 2: Slice from unleached sample of $SrCrO_4$ in epoxy. There are several levels of contrast including the $SrCrO_4$ particles, the epoxy and epoxy which is slightly darker (lower absorption).

Figure 3: (a) secondary and (b) backscattered images of a $SrCrO_4$ particle embedded in epoxy prior to any leaching experiments. (c) Secondary and (d) backscattered images of a different $SrCrO_4$ particle embedded in epoxy after leaching. Note the sharp well defined crystal structure of the $SrCrO_4$ particle prior to leaching whereas the particles after leaching have rounded edges and surrounding void space.

Figure 4: Top: Slice of a sample containing $SrCrO_4$ and $CaSO_4$ before (left) and after (right) leaching in 0.1M NaCl solution. Bottom: Slice with 3D distribution of $SrCrO_4$ particles above it before (left) and after (right) leaching. A scratch has been created at the surface of the sample near the $CaSO_4$ particle which was fully dissolved after the leaching experiment. All the $SrCrO_4$ particles have been dissolved around the $CasSO_4$ particle as indicated by the blue circle (top leached) and blue volume (bottom leached). Leaching was performed in 5% NaCl solution for 24h.

Figure 5: Models reported in the literature for heterogeneous pathways through coatings. (a) Heterogeneity introduced through layering including two separate layers (left) or gradients (right). (b) Lateral heterogeneity through pathways created in the presence of additive particles, in this case where PVC > CPVC so there is not enough polymer to fill the interstitial volume between all particles. (c) Penetrative (to the underlying metal) and non-penetrative pathways within the polymer (no additives). (d) Inhibitor particle clusters which lead to penetrative channels when exposed to water, which may end up with concentration gradients of inhibitor, corrodents and metal ions.

Figure 6: Matching stages of cluster dissolution with EIS equivalent circuits normally used to describe coatings at different stages of degradation. Exposure times on left are for the epoxy system studies here [15]. The equivalent circuits and times shown on the right have been taken from [43].

Figure 7: Schematic for several possible equivalent circuits based on individual structures observed using CT. Heterogeneous pore networks include the LDE (top), $SrCrO_4$ clusters (2nd from top), mixed pore networks involving water penetration partially through the polymer and partially through other pore networks ($SrCrO_4$ or LDE) (3rd from top) and the epoxy itself (bottom).

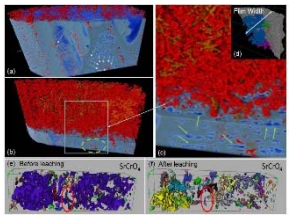

Figure 1

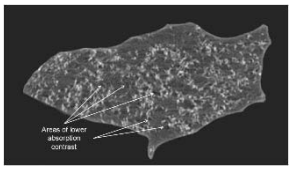

Figure 2

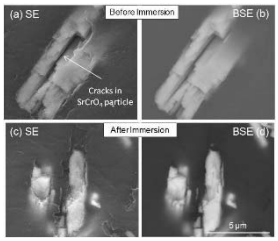

Figure 3

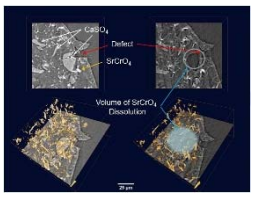

Figure 4

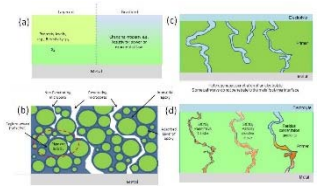

Figure 5

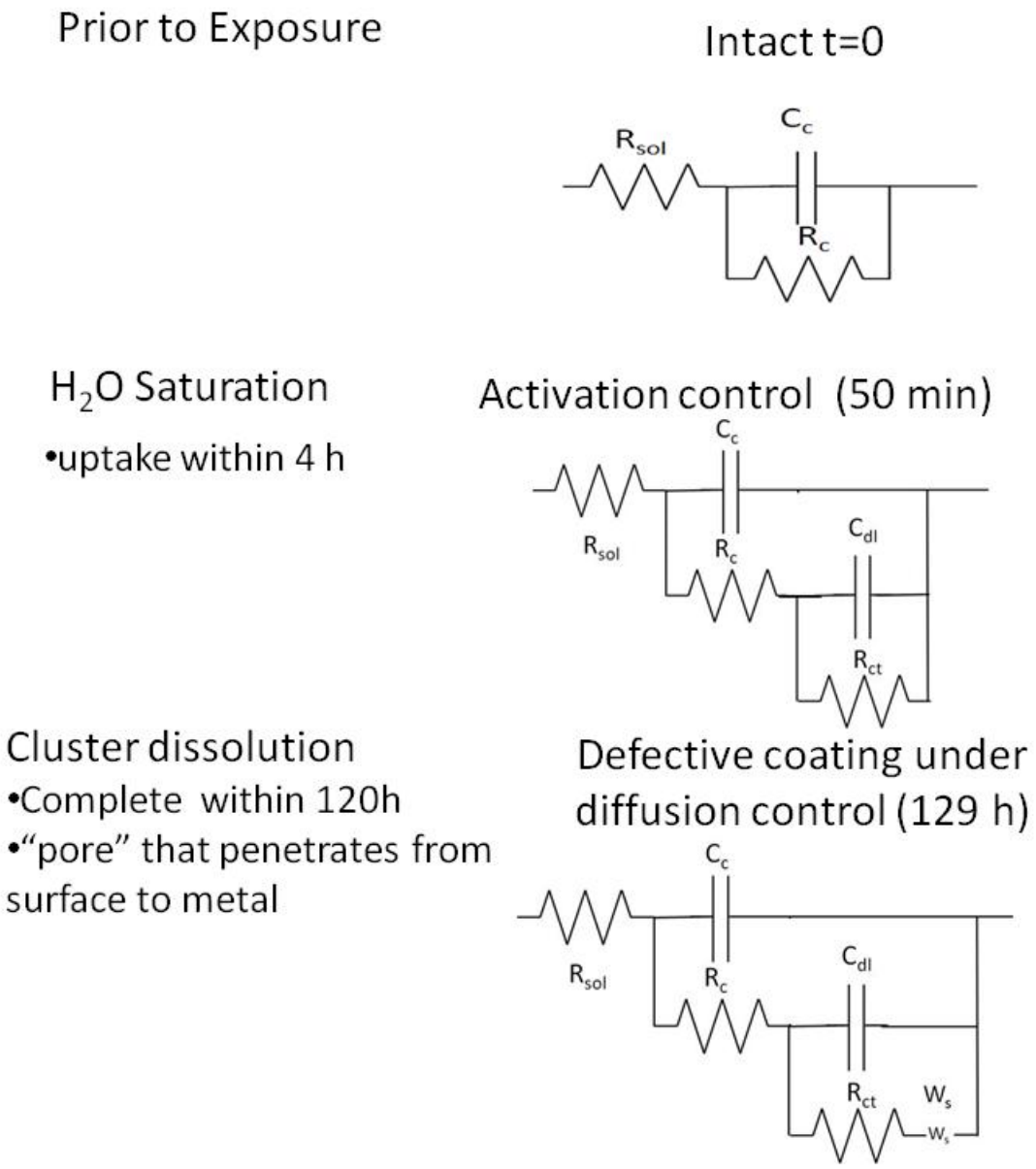

Figure 6:

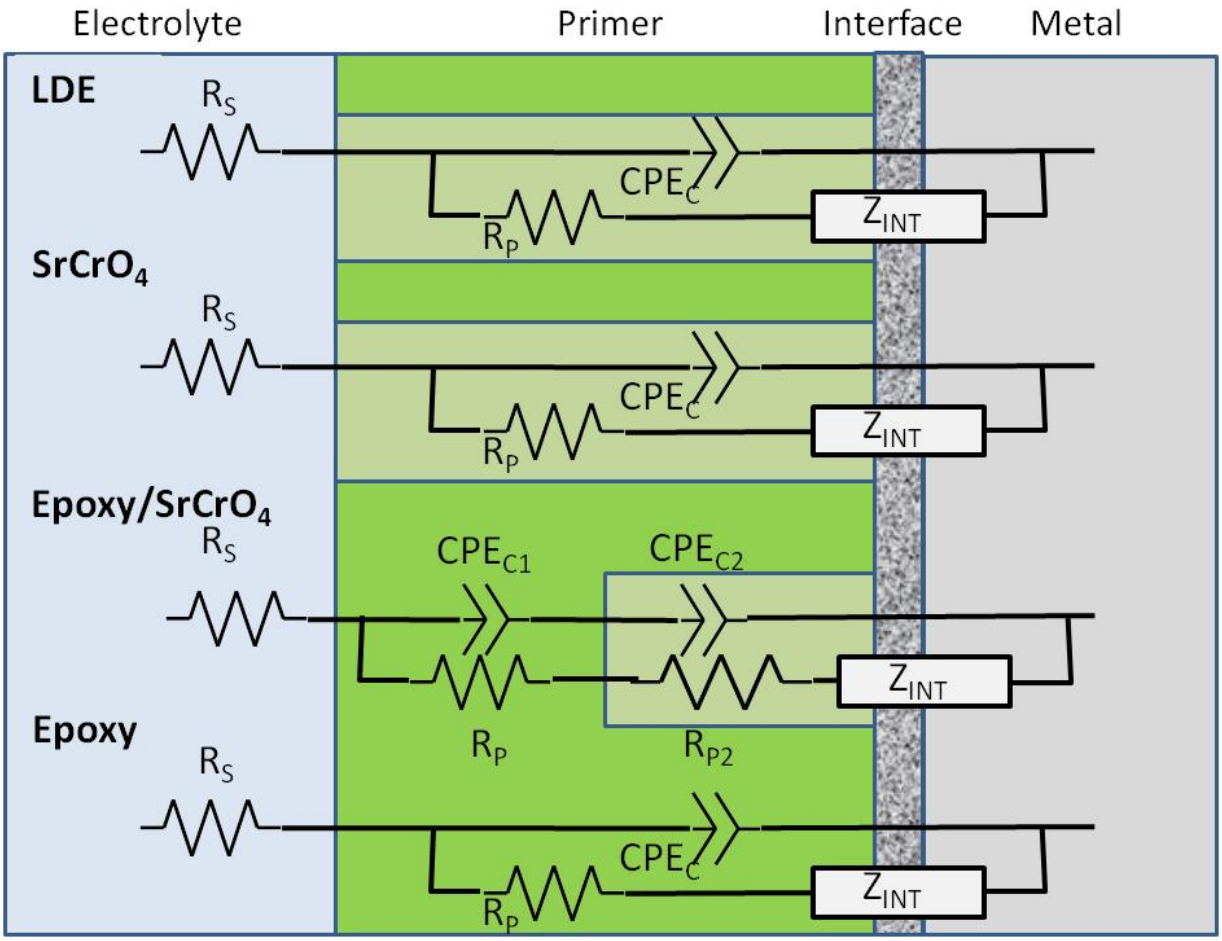

Figure 7

Table 1: Inhibitor Sizes (Data taken largely from [56]for M-O and [57] for C-C and C-O bonds)

Inhibitor	**Characteristic Size (Å) without waters of hydration***
Chromate (CrO_4^{2-})	3.2 (condensation in acid environments)
Molybdate	3.6 (polymerization in acid environments)
Vanadate	3.6 (mononuclear species at low or high pH, but polynuclear at intermediate pH [56, 58])
Phosphate	3.3
Polyphosphates	Large, but the P-O-P can hydrolise in acidic solution
Organophosphate	Depends on ligand. The following are the size of the ligand: OButyl: 5.8 OPhenyl: 4.2
Mercaptobenzotirazole	5.6 (characteristic length based on the square root area)
Polymer System	**Reported Pore Volume**
Epoxy no additives different curing agents [59]	2.7 – 2.8
Polyimide [22]	3.27
Polyimide [60]	3.2 and 3.75 (bimodal)
Epoxy [15]	5.5

* Size determined using the M-O bond length unless otherwise stated.